Materials and Structures (2022)55:138
https://doi.org/10.1617/s11527-022-01978-w

ORIGINAL ARTICLE

Self-sensing asphalt composite with carbon microfibers for smart weigh-in-motion

Hasan Borke Birgin · Antonella D'Alessandro · Alessandro Corradini · Simon Laflamme · Filippo Ubertini

Received: 9 December 2021 / Accepted: 2 May 2022

Abstract The need for ageing infrastructure monitoring has recently emerged as an urgent priority in many countries. Smart road infrastructure is a technology that could be used to address this issue by enabling on-time decisions such as condition-based maintenance. For example, automatic traffic monitoring could be beneficial by improving fatigue analysis, and maintenance priority planning and management of overloaded vehicles. This can be done through image-based traffic monitoring, weight measurements by static scales, and weigh-in-motion (WIM) stations. WIM can be used to identify and classify the type, the number, and the weight of vehicles passing over a given road segment without interrupting the traffic flow. The general drawbacks of existing WIM technologies are their high costs, low durability, and complex deployment. This paper proposes a new asphalt-like composite enabling self-sensing road pavements that can serve as a low-cost and durable WIM sensor. The proposed novel material consists of a commercial binder called EVIzero, doped with natural aggregates and carbon microfibers. These microfibers provide electrical conductivity and piezoresistive properties through electrical percolation. Here, both the material preparation for road applications and its electromechanical characterization are examined. Various cylindrical samples fabricated using different percentages of carbon microfibers were produced and investigated in order to evaluate their signal quality and strain sensing capabilities. It is found that the material mix fabricated with 1% carbon microfibers with respect to the binder weight has the best sensing performance due to electrical percolation. A mid-size slab sample is produced using this optimal mix in order to achieve a preliminary demonstration of material's feasibility for WIM sensing. The results show that a linear relationship between the electrical response of the slab sample and the induced strain is established with an R^2 of 93%.

H. B. Birgin (✉) · A. D'Alessandro · A. Corradini · F. Ubertini
Department of Civil and Environmental Engineering, University of Perugia, via Goffredo Duranti 93, 06125 Perugia, PG, Italy
e-mail: hasanborke.birgin@unipg.it

A. D'Alessandro
e-mail: antonella.dalessandro@unipg.it

A. Corradini
e-mail: alessandro.corradini@unipg.it

F. Ubertini
e-mail: filippo.ubertini@unipg.it

S. Laflamme
Department of Civil, Construction, and Environmental Engineering, Iowa State University, Ames, IA 50011, USA
e-mail: laflamme@iastate.edu

Published online: 19 May 2022

Keywords Smart weigh-in-motion · Road monitoring · Carbon micro fibers · Composites · Self-sensing material

1 Introduction

Technological improvements over the last decades have encouraged the development of advanced sensing technologies for structural health monitoring (SHM) of ageing infrastructures. Yet, numerous challenges are impeding their widespread applications, including their relative high costs, uncertain durability, and complex installation. To address some or all of these issues, smart self-sensing structural materials capable of strain sensing have gained in popularity [1, 2]. In particular, they are highly durable, with a lifetime associated with that of the base structural material [3]. Also, the transducer is perfectly bonded with the structure through the direct integration of the sensing mechanism with the structural material. It follows that the maintenance of these materials is limited during their operation time [4]. In addition, it is foreseen that the fabrication cost of self-sensing materials will decrease significantly in a near future due to progress made in micro- and nano-fillers, encouraging more field applications and thus potentially leading to increased structural safety [5, 6].

Smart materials can be employed over large volumes or areas to provide multi-functionalities that include strain sensing capabilities [7–11]. Strain sensors made from self-sensing materials exploit the piezoresistive effect that produces a detectable and repeatable variation of the electrical resistance as a function of strain. At low levels of strain, such as those experienced in civil structures, the relative change in resistance is proportional to the level of strain. This proportionality is called the gauge factor of the sensor. By leveraging the piezoresistive effect, the gauge factor of self-sensing materials can be orders of magnitude higher than those of conventional resistive strain gauges [12]. Generally, self-sensing materials are fabricated through the dispersion of electrically conductive inclusions inside an insulating binder matrix [13], for which carbon fillers are of high interest because of their high electrical conductivity compared to the binder matrix of asphalt concretes used in road pavements. Electrical conductivity of composites is provided through the formation of conductive paths [14]. The composite electrical conductivity increases significantly when a concentration level is exceeded, which level depends on the conductivity of inclusions. This level defines the electrical percolation threshold of the specific filler within a matrix material. Under compressive or tensile strains, the conductivity of the smart material can vary greatly due to the variation in inter-particle distances, the deformations of the conductive particles, the variation of contact resistances between fillers and binder matrix, and other field effects [15].

When dispersing small amounts of conductive fillers, the contribution of particles in terms of conductivity remains limited. Body deformations under induced strain are expected to play a major role in the variation of resistance, thus the electrical response of the material is susceptible to noise and drift due to polarization. Dispersing an excessively high amount of fillers over the electrical percolation threshold can cause the material matrix to turn into an electrically conductive material, where the electrons can travel through the material via a conductive network formed by only carbon inclusions. Change in the inter-particle distance, in this case, will not have a significant effect on the conductivity of the composite material, which implies a reduced gauge factor or loss of strain sensitivity. Literature discussed optimum level of carbon additives where the strain sensitivity of the carbon-doped composite reaches its maximum amount [16]. Often, this optimum level is near the electrical percolation threshold of the material, where the material encounters a transition from being an electrical insulator to an electrical conductor. The optimum levels of doping depend on the matrix material, as well as on the type and the morphology of inclusions. This level may be revealed by experimental tests supported by numerical and analytical computations according to percolation theory [17–20].

For SHM applications, a strain sensor should provide a stable electrical signal without being affected by noise and drifts. Literature counts many researches on the reliability of self-sensing cementitious and clay-based composites [21–25]. The studies demonstrate sensing performances that are appropriate for SHM applications. An issue may be with dispersion, in particular if the inclusions dispersed within the composite matrix are nano-sized which can easily yield agglomerations. Recent research on scalable

smart composites has shown new possibilities for wide production and application [26]. For detecting static loads and obtaining strain field through measurements taken by the load-bearing structural elements, both cement and clay-based composites are promising sensors [27, 28]. However, their usage is limited when detecting high-rate dynamic loads, such as those produced by traffic loads. This is due to the utilization of biphasic input voltage to cancel out the polarization of such types of composites. Accordingly, on the output side, the signals should be downsampled, thus restraining the time resolution [29]. In addition, stable biphasic inputs require cost-demanding instrumentation. Using a DC Voltage as a solution creates polarization drift that leads to inaccuracy when scaling the loads.

In this study, a new asphalt composite material is proposed for sensing dynamic traffic loads on road infrastructures such as bridges and viaducts [30]. The intended application is WIM sensing. Existing WIM technologies are typically based on embedded piezoelectric sensors, which have high costs and limited life spans. The material investigated in this study is aimed at providing a low-cost and high durability alternative. It is composed of a new commercially available sustainable binder material called EVIzero (Corecom srl. [31]), natural aggregates, and carbon microfibers (CMF, SGL Carbon [32]). In the study, cylindrical samples with 10 cm diameter and 6 cm height including 0%, 0.5%, 1%, 1.5%, 2%, 2.5%, 3%, 4%, 5% of fibers with respect to the weight of the binder are investigated for their electrical resistivity and strain sensing capabilities. A mid-size slab sample of dimensions $40 \times 30 \times 4\,\text{cm}^3$ is fabricated using the most performing mixture. The slab is instrumented by multiple embedded copper line electrodes and tested for load and strain sensing capabilities.

The rest of the paper is organized as follows. Section 2 introduces the samples produced for the study. Section 3 discusses the piezoresistive models of the samples, depending on their geometries, and introduces testing methodologies. Section 4 presents the results on the percolating behavior of the material and the load sensing performance of the cylindrical samples, reveals the best performing material mixture, and inspects the sensing ability of the slab sample. Section 5 discusses the findings of the study and the possible field applications. Section 6 concludes the paper.

2 Materials and samples preparation

The study aims at developing a reliable material design that has piezoresistive sensing capabilities. The performance tests conducted on the composite material are: (i) assessment of dispersion quality and definition of percolation threshold using small-scaled cylindrical samples; (ii) optimization of composite design through analysis of gauge factor and sensing quality by conducting electro-mechanical tests on cylindrical samples; (iii) evaluation of composite scalability to larger dimensions using a plate sample of bigger dimensions; (iv) electro-mechanical tests on the plate sample to perform load localization and scaling, and assessment of sensing reliability.

The materials of the study are eco-friendly EVIzero binder by Corecom s.r.l [31], carbon microfibers from SGL Carbon [32], and Ancona Bianco aggregates obtained from SINTEXCAL s.r.l. EVIzero is a neutral-colored binder based on polyolefin, made with polymers and industrial by-products. The carbon microfibers are cut carbon fibers with a single fiber length of 6 mm and a diameter of 7 μm. The single filament resistivity is reported as 15 μΩm by the producer and is thus suitable for enhancing the electrical properties of the composite matrix. Table 1 lists the material characteristics.

The production process of the proposed novel pavement material is similar to the one of bitumen road asphalt. The amounts of materials used for cylinders for each type of mixture are presented in Table 2.

A cylindrical sample is produced under each material mixture. The concentration levels of CMF in terms of weight ratio to EVIzero are 0%, 0.5%, 1%, 1.5%, 2%, 2.5%, 3%, 4% and 5% CMF/EVIzero. The ratio in weight CMF/EVIzero adopted for the slab sample is 1%. This concentration, as it will be discussed in the results section, is determined as the most performing mixture in terms of strain sensing sensitivity. The materials and amounts used for the slab sample are presented in Table 2.

The main fabrication phases are (i) preparation and heating of the material, (ii) mixing, and (iii) compaction. Figure 1 illustrates the production steps.

Table 1 Material characteristics for EVIzero [31], CMF [32] and copper

	EVIzero	CMF	copper
Conductivity (S/m)	–	6.67×10^4	58.7×10^6
Density (g/cm^3)	0.85	1.80	8.96
Softening point (°C)	75	3600	1085
Mixing temperature (°C)	160–170	–	–
Dynamic viscosity at 160°C (mPa·s)	700	–	–

Table 2 Mix designs of the composite material under each CMF/EVIzero doping level for the cylidrical and the slab samples

Doping level (%)	Cylindrical samples									Slab
	0.0	0.5	1.0	1.5	2.0	2.5	3.0	4.0	5.0	1.0
Fine aggregates w. (g)	627	627	627	627	627	627	627	627	627	5745
Coarse aggregates w. (g)	573	573	573	573	573	573	573	573	573	5255
EVIzero w. (g)	75	75	75	75	75	75	75	75	75	680
CMF w. (g)	0.00	0.38	0.75	1.13	1.50	1.88	2.25	3	3.75	6.80

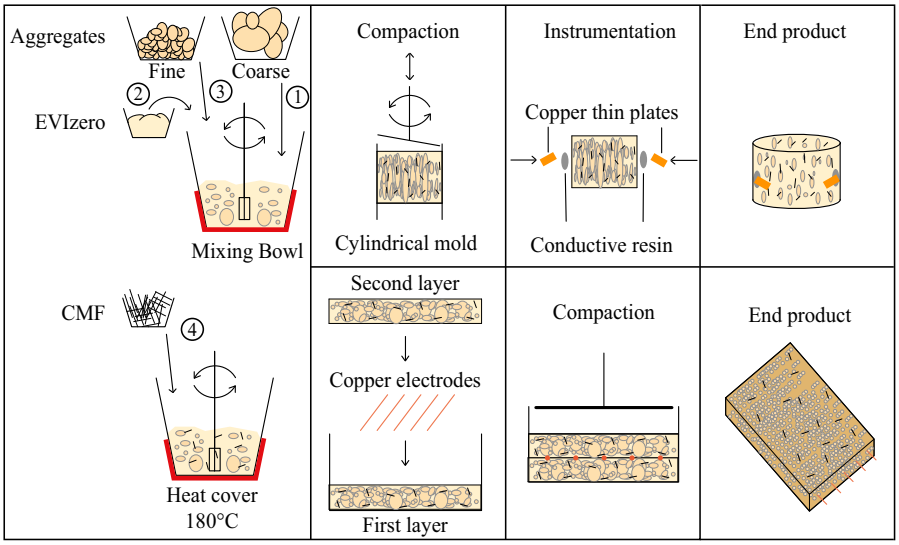

Fig. 1 Samples fabrication procedures illustrated step-wise

During the process, 0–4 mm sized fine aggregates and 4–8 mm sized coarse aggregates are prepared separately in two metal trays. The aggregates mix design as presented in Table 2 complies with the minimum and maximum design gradation curves using 0–8 mm sized aggregates defined by the experimental characterization study of EVIzero mixtures for pavements [33]. The aggregates in given amounts are put inside the oven under 180°C for 3 h. EVIzero and other mixing tools, including iron mixing bowl, metal shovels, and molds are heated at 180°C for 1 h before mixing. The heating at 180°C is used for compensating the expected heat losses at the surfaces and to assure the ideal mixing temperature during the preparation process.

After all the materials reach the desired mixing temperature, hot coarse aggregates are poured inside the mixing bowl. Next, the desired amount of heated EVIzero is poured on top of hot coarse aggregates, followed by the addition of fine-sized aggregates. The mixture is mixed until homogeneity of the material is reached using a laboratory mixer. Then, CMF are added to the compound and mixed continuously until achieving their visually good dispersion. Inhomogeneous dispersion of CMF would lead to agglomerations and consequently an anisotropy of the composite,

which may significantly impair load sensing features. In this light, the proposed mixing method has been optimized and properly tailored after laboratory trials in order to reach a trade-off between practical feasibility and mixing quality, resulting in sufficiently repeatable and uniform electrical features of the composite material. Two different compactors are employed, namely gyrotary compactor: Controls group model 76-B0251 presented in Fig. 2a and the roller compactor: Controls group model 77-PV41A02 presented in Fig. 2b. Such devices are used for the production of cylinders and the slab complying with the guidelines for the compaction of traditional asphalt concrete mixtures in the laboratories UNI EN 12697-31 [34] and UNI EN 12697-33 [35], respectively. For the cylinders, the composite mixture is cast into a cylindrical mold of 10 cm diameter and compacted over 200 cycles achieving the final density approximating to 2.400 g/cm^3. Afterward, the compacted cylindrical sample is taken out of the mould and cooled down. When the sample temperature drops to ambient, it is instrumented using external electrodes and strain gauges.

The compaction methodology for the slab differs from that of the cylinders to allow for the placement of line electrodes inside the material. The mixed material is separated into two equally weighing batches that form the upper and lower layers of the sample. The dimensions of the layer surface area are $40 \times 30\,\text{cm}^2$. The electrodes are placed between two equally weighing material layers, and they remain in the middle of the thickness after the compaction. The compaction process continues until the uniform thickness of the slab sample becomes 4 cm, which corresponds approximately to a density of 2.400 g/cm^3. After the cooling down, the slab is instrumented with a strain gauge (Fig. 3) as described in details in the following sections.

3 Piezoresistive models and testing methods

3.1 Piezoresistivity of cylindrical samples

Figure 4 shows the dimensions and instrumentation of the produced cylinders of the study. Accordingly, the cylindrical samples shown in Fig. 4a have four horizontal, external copper-sheet electrodes attached to the side surface with conductive resin made from graphite powder and a bi-component epoxy resin having the graphite weight concentration of 75%. The electrodes are placed at 90° in the plane. During the compression tests, the induced strain is measured using LVDTs. In order to calibrate the readings with

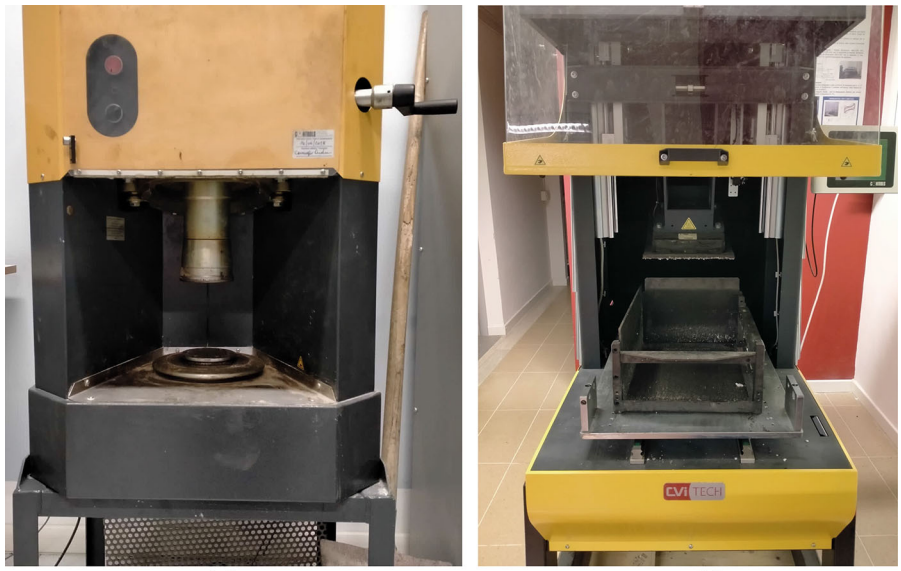

Fig. 2 Compactors used for the study; **a** compactor to fabricate cylindrical samples (Controls group model 76-B0251); **b** compactor to fabricate the slab sample (Controls model 77-PV41A02)

Fig. 3 The tested samples during the study; **a** cylindrical samples; **b** slab sample

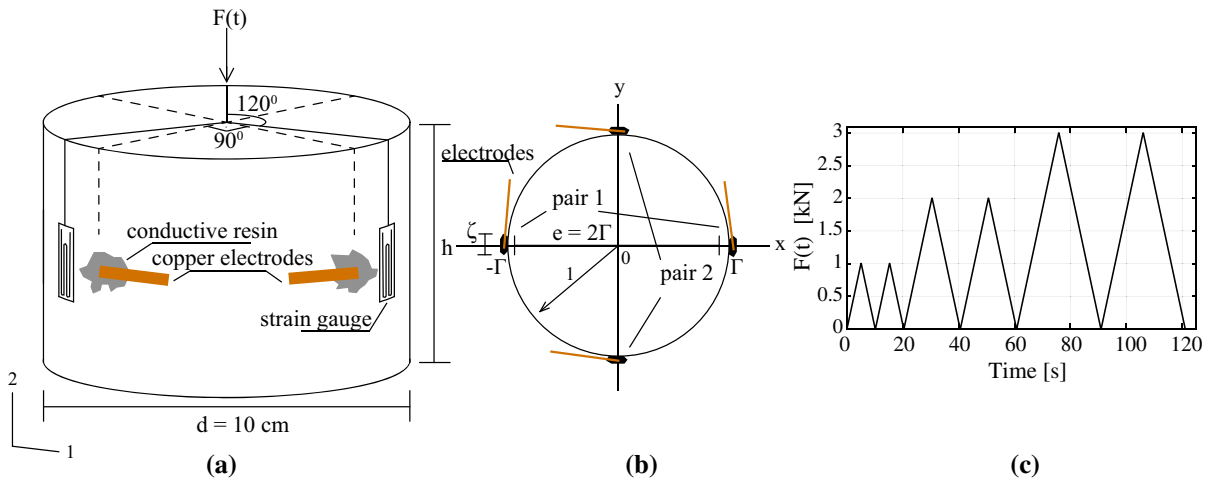

Fig. 4 Sketch of the cylindrical sample; **a** general 3D view with samples instrumentation applied force direction, and related dimensions and directions; **b** the top view of samples showing the spatial variables for calculations of resistance and piezoresistivity; **c** the compressive load pattern adopted for cylindrical samples

LVDTs, selected samples are instrumented with three monoaxial 2-cm strain gauges with a 120 Ω sensor resistance and a gauge factor of 2.1, placed at 120° in the plane to measure the strains in the vertical direction (ε_2).

Piezoresistive behavior of cylindrical shapes as illustrated in Fig. 4b is formulated by adapting the general solution of McDonald [36] to the resistance of a disc problem. The cylindrical samples of this study are particular cases of the disc model used in the reference. Accordingly, R denotes the resistance, ρ the resistivity, t the thickness, Γ the radius of the disc, 2Γ the diameter (secant distance between opposite electrodes), and ζ the width of electrodes. Based on this model, resistance is formulated as follows:

$$R = \frac{2\rho}{\pi t} \ln \frac{4\Gamma}{\zeta} \tag{1}$$

where the uniform thickness of the disc is denoted by t. Taking the total differential of the above-given formulation, the following Equation is attained.

$$\mathrm{d}R = \frac{2}{\pi t}\,\mathrm{d}\rho \ln \frac{4\Gamma}{\zeta} - \frac{2\mathrm{d}t}{\pi t^2}\,\rho \ln \frac{4\Gamma}{\zeta} + \frac{2}{\pi t}\,\rho\,\frac{\mathrm{d}\Gamma}{\Gamma} \tag{2}$$

Followed by division to R, fractional variation of resistance is expressed as follows.

$$\frac{\mathrm{d}R}{R} = \frac{\mathrm{d}\rho}{\rho} - \frac{\mathrm{d}t}{t} + \frac{\mathrm{d}\Gamma}{\Gamma}\frac{1}{\ln(4\Gamma/\zeta)} \tag{3}$$

Recalling sample model in Fig. 4a, and considering Poisson's effect ($\varepsilon_1 = -v\varepsilon_2$), Eq. 3 yields into:

$$\frac{\mathrm{d}R}{R} = \frac{\mathrm{d}\rho}{\rho} + \frac{\varepsilon_1}{v} + \varepsilon_1 \frac{1}{\ln(4\Gamma/\zeta)} \tag{4}$$

and the gauge factor is expressed as:

$$\lambda_c = \frac{\frac{\mathrm{d}R}{R}}{\varepsilon_1} = \frac{\frac{\mathrm{d}\rho}{\rho}}{\varepsilon_1} + \left(\frac{1}{v} + \frac{1}{\ln(4\Gamma/\zeta)}\right) \tag{5}$$

where both v and $4\Gamma/\zeta$ are positive quantities given $\Gamma \gg \zeta$. The expression for the gauge factor includes three terms: (i) the fractional change in resistance, $\mathrm{d}R/R$, that is the directly observable term that is measured during the electro-mechanical tests; (ii) the fractional change in resistivity, $\mathrm{d}\rho/\rho$, that is the feature of the material that is alterable by the mixture design; and (iii) the rest of the equation that represents the variations due to the body deformations.

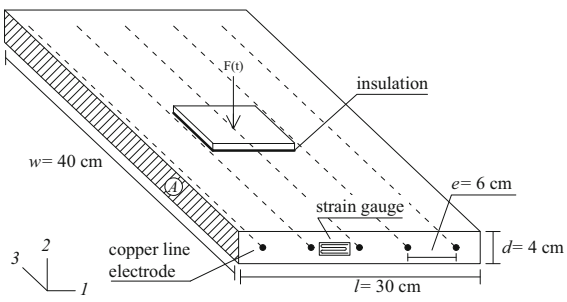

Fig. 5 The instrumented slab sample investigated in the study: dimensions and loading scheme

3.2 Piezoresistivity of slab sample

The slab sample shown in Fig. 5 has five internal copper wire electrodes, placed at a mutual distance of 6 cm. In the given configuration, the resistance between the electrodes can be written by the following equation having the cross-sectional area between the electrodes constant:

$$R = \rho \frac{L}{A} \tag{6}$$

where L is the distance between electrodes and A is the cross sectional area. The differentiation of the equation yields:

$$\frac{\mathrm{d}R}{R} = \frac{\mathrm{d}\rho}{\rho} + \frac{\mathrm{d}L}{L} - \frac{\mathrm{d}A}{A} \tag{7}$$

$$\frac{\mathrm{d}R}{R} = \frac{\mathrm{d}\rho}{\rho} + \frac{\mathrm{d}l}{l} - \frac{\mathrm{d}d}{d} - \frac{\mathrm{d}w}{w} \tag{8}$$

$$\frac{\mathrm{d}R}{R} = \frac{\mathrm{d}\rho}{\rho} + \varepsilon_1 - \varepsilon_2 - \varepsilon_3 \tag{9}$$

where the dimensions l, d, w are indicated in Fig. 5. Recalling the notation in Fig. 5, knowing that the loading is in direction-2, and using the conversion $\varepsilon_1 = -v\varepsilon_2$, the equation can be written in terms of strain that corresponds to direction-1 (ε_1):

$$\frac{\mathrm{d}R}{R} = \frac{\mathrm{d}\rho}{\rho} + \varepsilon_1 + \frac{\varepsilon_1}{v} - \varepsilon_1 \tag{10}$$

$$\frac{\mathrm{d}R}{R} = \frac{\mathrm{d}\rho}{\rho} - \frac{\varepsilon_1}{v} \tag{11}$$

Dividing Eq. 11 by ε_1, the governing equation for electro-mechanical tests becomes:

$$\lambda = \frac{\frac{\mathrm{d}R}{R}}{\varepsilon_1} = \frac{\frac{\mathrm{d}\rho}{\rho}}{\varepsilon_1} + \frac{1}{v} \tag{12}$$

where now the term relating to the body deformation is simpler than the one of cylindrical shape. This is due to the simplicity obtained through the uniform cross-section and the electrodes' geometry.

3.3 Measurement hardware and sensing schemes

The samples made of the newly developed composite are subjected to electromechanical tests. The tests reveal the conductivity of the material as well as its

load sensing performance. The mechanical part of the tests comprises cyclic compression loads. Together with the compression load time history, the induced strain time history is recorded for evaluating the gauge factor of the samples. The electrical part of the tests consists of resistance measurements of the samples using their electrodes. The tests establish the correlation between strain and resistance according to the equations presented in previous sections. The performance is qualified based on the linearity of the correlation and gauge factor.

For the above-given purposes, two types of circuits are designed for resistance recordings. The electrical circuit presented in Fig. 6a is adopted for electromechanical tests on cylinders and on the slab sample. This electrical circuit consists of a shunt resistor connected in series to the inspected sample. The electrical circuit has a DC voltage input. The time histories of voltage variations through the shunt resistor and the sample are measured and recorded by the DAQ. Then, the resistance time history, $R(t)$, is calculated by simple Ohm's law, using the voltage time histories:

$$R(t) = \frac{V_s(t)}{V_k(t)} \cdot R_k \tag{13}$$

where V_s and V_k are the voltages measured through sample and shunt resistor, respectively. R_k is the selected resistance value for the shunt resistor. In this study a $1000\,\Omega$ resistor is used for both types of samples. The circuit shown in Fig. 6c is adopted only for the slab sample to create waveform WIM signals compatible with the reference study [30]. In that configuration, the voltage time histories are being read through two subsequent volume segments of the slab. Their difference creates a time history that is a waveform and exhibits peak amplitudes scaled to the position and magnitude of moving loads. Such difference is taken as:

$$\Psi(t) = V_1(t) - V_2(t) \tag{14}$$

where $\Psi(t)$ is the obtained waveform time history, while $V_1(t)$ and $V_2(t)$ are the voltage readings through 1st and 2nd segments, respectively. The 5V DC voltage input and data acquisition of the designed circuits are carried out using a National Instruments (NI) PXI. A PXIe-4138 is used for sourcing the steady DC Voltage and a PXIe-4302 is used as an analog to digital converter for voltage readings. For applying the cycling loads on the cylindrical samples, Advantest 50-C7600 by Controls with a maximum load of 15 kN is employed. The strains of the cylinders are measured by three high-precision LVDTs placed at 120° in plane. The slab sample is loaded by a manually controlled hydraulic press with a load capacity of 20 tons. The load is measured by a LAUMAS load cell with a reading capacity of 10 tons. The slab sample is instrumented with a strain gauge placed between 2nd and 3rd electrode ends on the frontal side in the horizontal position to provide a measure of deformation during the tests. Data acquisition of all strain gauges is carried out by a PXIe-4330. All the related processes are developed and recorded under a NI-LABVIEW environment.

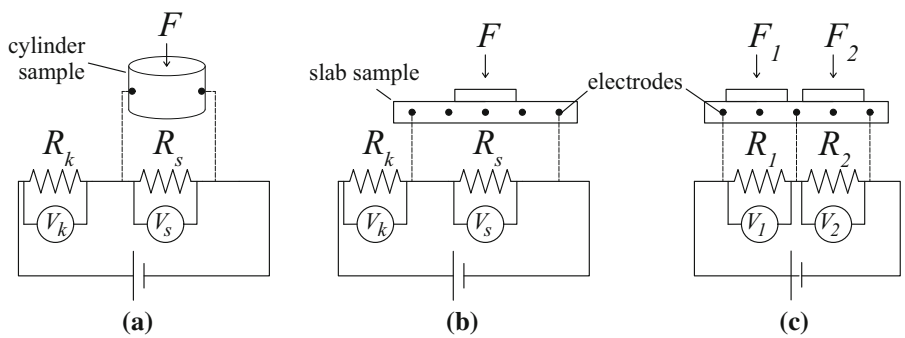

Fig. 6 The test setups and their equivalent electric circuits adopted for the electromechanical tests; **a** tests conducted on cylinder; **b** fast and slow varying load tests on the slab sample; **c** varying location load test on the slab for WIM sensing suitability

4 Results

4.1 Percolation analysis

The analytical percolation model developed by the available studies in the literature [37–39], can be adopted for the given type of material and fillers. When dispersed adequately, the fibers inside the EVIzero matrix behave as electrically conductive fillers in a void. The adopted analytical model of Fig. 7a shows the curve of the volumetric fraction of fillers at percolation threshold as a function of the aspect ratio of fillers. This curve is plotted together with corresponding weight ratios of CMF/EVIzero, where conversion from weight ratio of fillers to the volumetric fractions of fillers has been carried out by taking the cylindrical sample geometry and material densities into account. The aspect ratio of CMF is close to 900 according to the dimensions presented in the datasheet of the product [32].

Inspecting the curve in Fig. 7a, the 1% CMF/EVIzero weight ratio can be observed as having critical volumetric fraction, consistent with the aspect ratio of the fillers. To verify this result, experimental percolation has been evaluated considering the average resistance of cylinders between two laterally opposing electrodes. The readings are plotted against CMF/EVIzero weight fractions in Fig. 7b. Results indicate that the sample containing 1% CMF/EVIzero weight ratio approximately coincides with the transition zone of the composite from being an electrical insulator to becoming an electrical conductor, indicating that the electrical percolation threshold of CMF is around such a concentration level. It is concluded that the experimental readings verify the analytical model, and 1% CMF/EVIzero stands out as the most promising doping level.

4.2 Performance evaluation of cylindrical samples

The suitability of the proposed self-sensing composite is examined for WIM sensing application by inspecting the correlation between induced strain and variation of samples' electrical resistance. Figure 4c depicts the adopted cyclic load pattern of the tests. Accordingly, two triangular cycles of three different maximum load levels are designed with peak increments of 1, 2, and 3 kN, corresponding to compressive stresses of 0.13, 0.26, and 0.39 MPa. The tests are repeated two times consecutively by using both electrode pairs, thus allowing the material to generate electrical responses starting from both relaxed and compacted initial conditions. The load increase is set to 200 N/s, allowing the sampling of various stress levels. The results of the electromechanical tests are presented in Figs. 8 and 9.

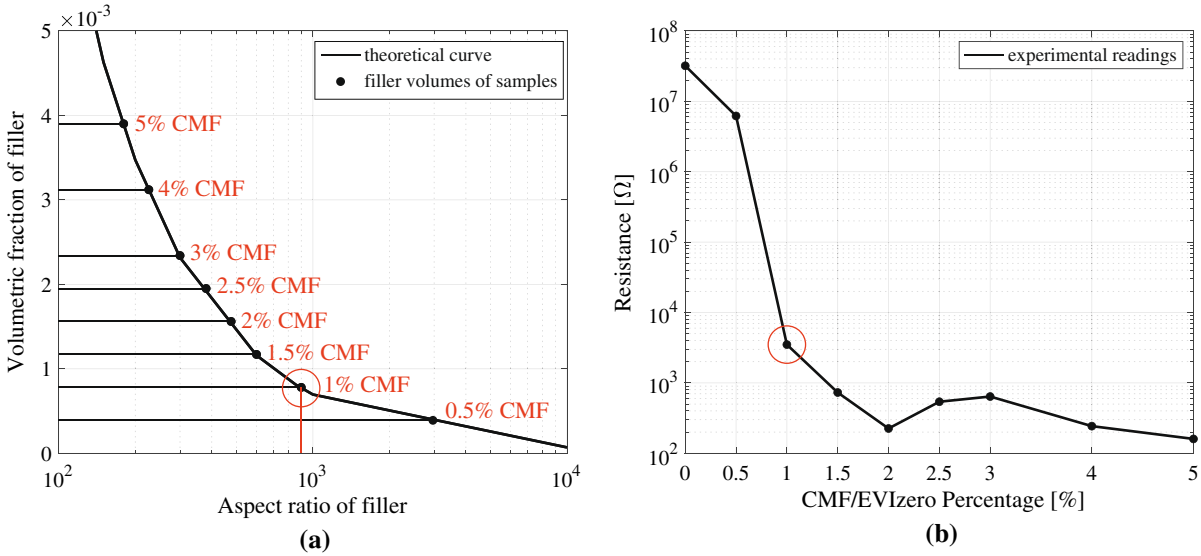

Fig. 7 The outcomes of analytical and numerical percolation threshold studies conducted on the cylindrical samples; **a** analytical model of critical volumetric fraction of fillers with respect to aspect ratio; **b** resistance readings of samples, showing that the 1% sample is in the transition zone

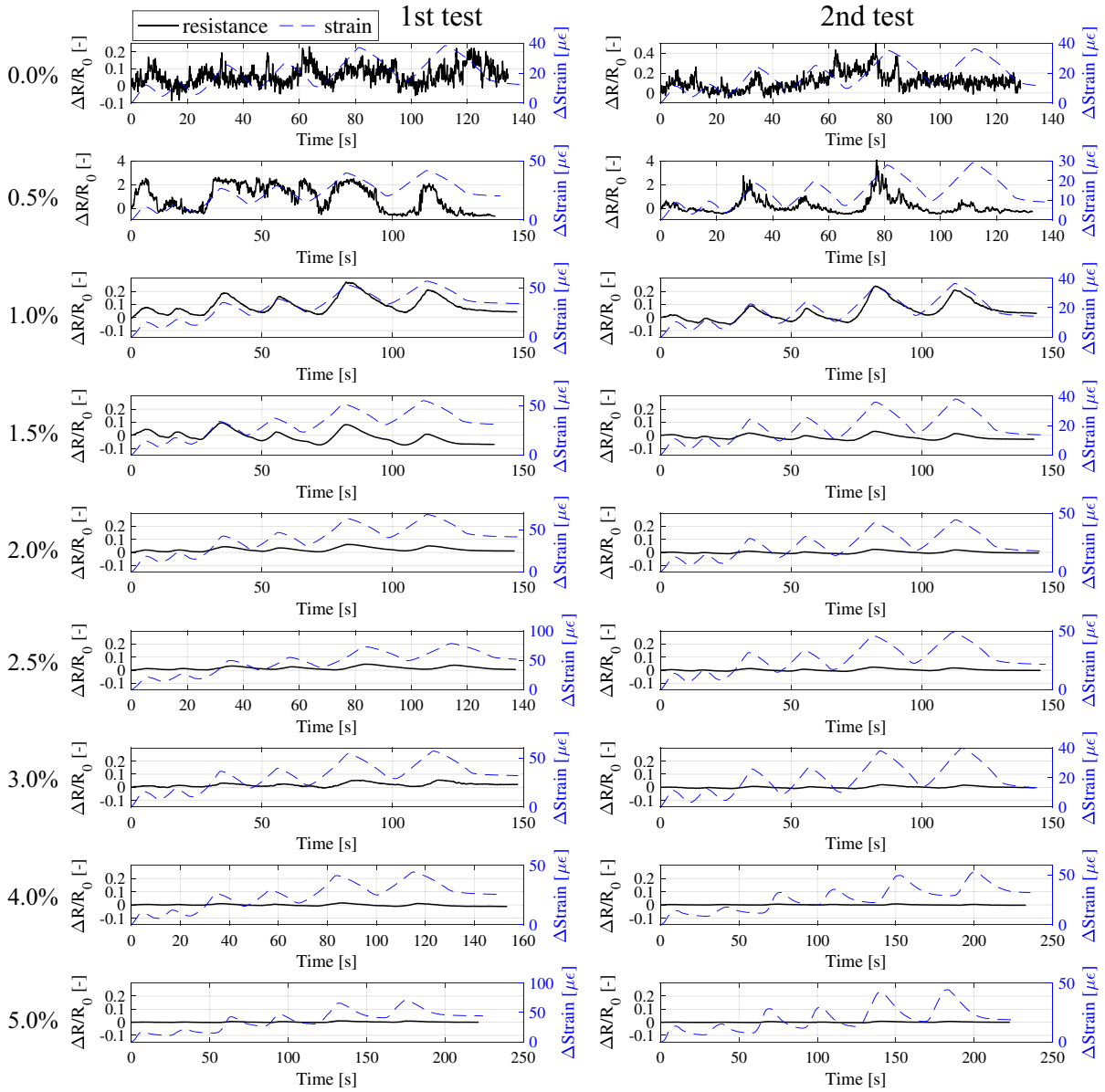

Fig. 8 Outcomes of electro-mechanical test performed on cylindrical samples. Strain and change of resistance time histories for samples doped with different amounts of CMF, from 0 to 5% with respect to the weight of the EVIzero

In Fig. 8, resistance and strain time histories are plotted together to compare the generated resistance response to the induced strain. Figure 9 shows the discrete data points and the linear fit models of the data.

The main findings from the results are as follows: (i) the responses initialized from relaxed state and compacted state differ in terms of residual drifts, this is attributable to the visco-elastic nature of the material; (ii) 1% CMF/EVIzero sample outperforms all other samples in terms of linearity and gauge factor value; (iii) evaluating the electric responses to the given load time history, with the increasing concentrations of CMF, the composite is found gradually losing its improved strain sensing ability when over-percolated due to the governing body deformations over piezoresistivity for the variation of sample resistance, as analytically discussed in the literature [39], and (iv)

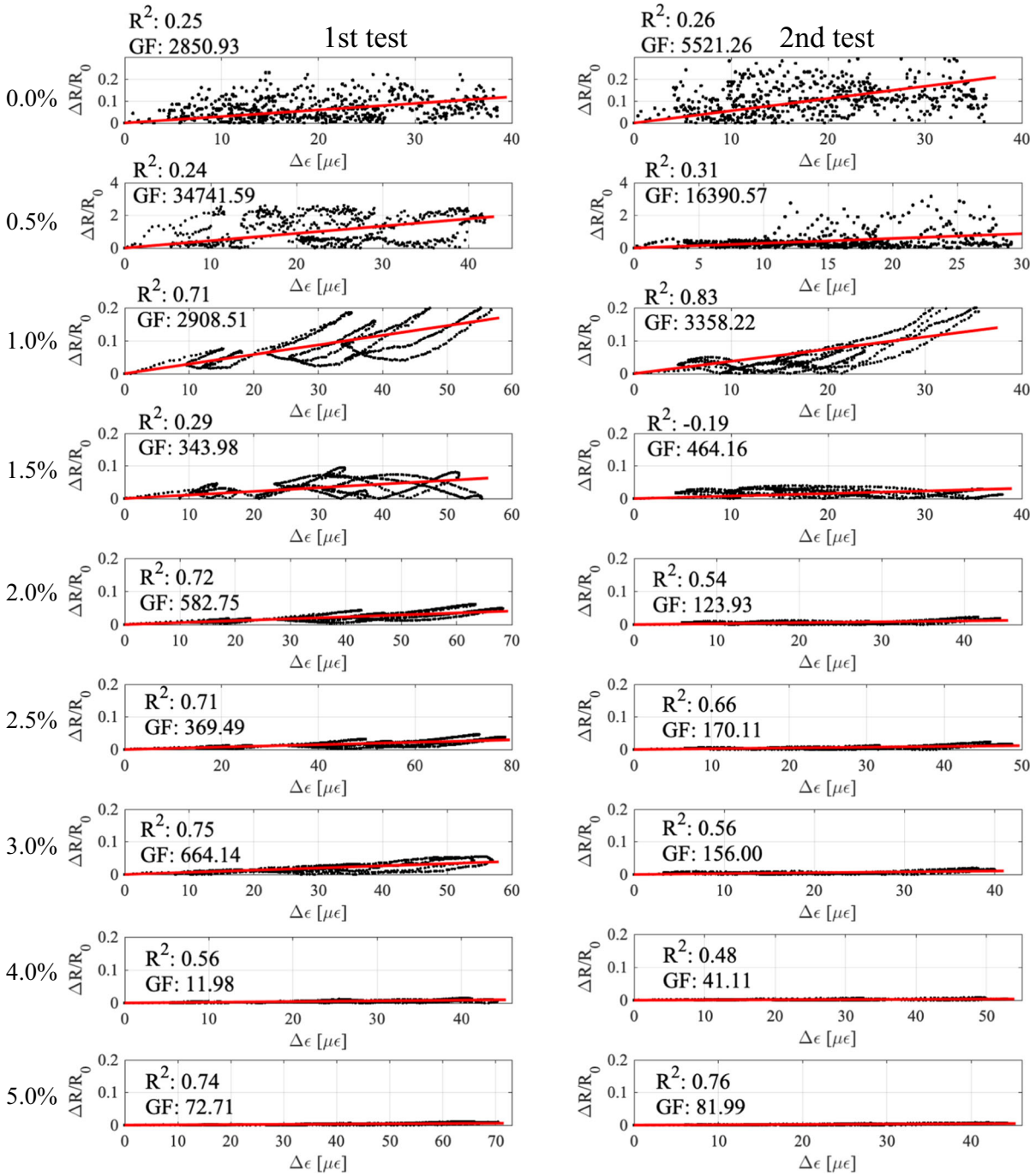

Fig. 9 Linear fits of the electro-mechanical tests on cylinders under various amounts of CMF up to 5.0%

the material can provide clean signals free from polarization drift despite being charged by DC voltage.

The results that are obtained through electromechanical tests on cylindrical samples demonstrate that the 1% CMF/EVIzero composite material is found very promising for the development and testing of larger scaled sensing units. The findings are summarized in Table 3.

Table 3 The outcomes from cyclic compression tests on cylindrical samples

Mixture index	Average λ	Average R^2
0.0% CMF/EVIzero	4186	26
0.5% CMF/EVIzero	25,500	28
1.0% CMF/EVIzero	3133	77
1.5% CMF/EVIzero	344	29
2.0% CMF/EVIzero	352	63
2.5% CMF/EVIzero	270	69
3.0% CMF/EVIzero	410	66
4.0% CMF/EVIzero	26	52
5.0% CMF/EVIzero	77	75

The results with negative R^2 are discarded

4.3 Load sensing capabilities of slab sample

The sensing performance of the mid-sized slab sample is investigated by conducting two types of experiments. First, step loads of different magnitudes and durations are applied onto the slab in the middle of the surface area. Second, the slab is subjected to subsequent compression step loads of equal amplitude positioned on different locations on the sample surface, intended to simulate the effect of moving load on the sample surface.

Figure 6b shows the test setup employed during the step load tests. The compression loads are applied to the slab surface through a metal plate with a $10 \times 10\,\text{cm}^2$ contact area. The metal plate is covered by an insulating tape so as not to affect the electrical measurements. During the step load tests, two different load time histories are adopted. They differ in terms of the duration of loaded periods. The load time history with fast step loads possesses short loaded periods. This type of loading serves to evaluate the material's ability to sense various load amplitudes. The slow step loads have a long period of loaded phase at two load magnitude levels. The periods of loads are 4 min each, in order to inspect the stability of readings.

The load time history and results obtained from the short period test are shown in Fig. 10. The measured strain and the variation of resistance are found highly correlated. The results obtained from long period tests are presented in Fig. 11.

Similarly, stable results are acquired, highly correlated to the measured strain. Further tests are carried out to examine if the slab is suitable for detecting moving loads. Figure 6c illustrates the corresponding test setup. After the first application of compression load F_1, a second load of equal magnitude and duration is applied at a different position on the slab (F_2). Figure 12a, b show the obtained voltage time histories through two different volumes during the test. Figure 12c shows the post-processed time history of Ψ calculated according to Eq. 14.

According to the obtained voltage time histories, the applied load creates two peaks with different signs that depend on the loads' position on the sample, allowing spatiotemporal measurements done by a single sensing unit. Furthermore, the generated signal responses show repeatability in voltage pulse amplitudes and transient behavior while the slab switches between the unloaded and loaded states. The residual shift observed during the period between the two loading events is attributed to the viscoelastic nature of the material, which vanishes after the application of the second load. This finding shows that the two equal forces can counterbalance the occurring residual deformations if applied on the opposing sides of the central electrode. These findings also stress the necessity of having a good pavement material design that increases the elasticity to improve the reliability of measurements. Nevertheless, the post-processed time history of Ψ exhibits the anticipated characteristics required for a WIM characterization that has been studied in [30]. Therefore, the result of this test is promising for possible field verification of WIM by employing CMF-EVIzero composite materials.

5 Discussion and outlook

The study investigated a novel self-sensing pavement composite to be employed as a traffic sensing system. The main benefits of such design are the important reduction in sensor costs and increased durability of the sensing system. Because the novel composite is similar to the base pavement material, the sensor is expected to exhibit similar durability. The total cost of one pavement sensor and related electronic circuit for data acquisition is estimated to be as low as the 10% with respect to traditional piezoelectric sensor commonly used in the form of embedded sensing bars

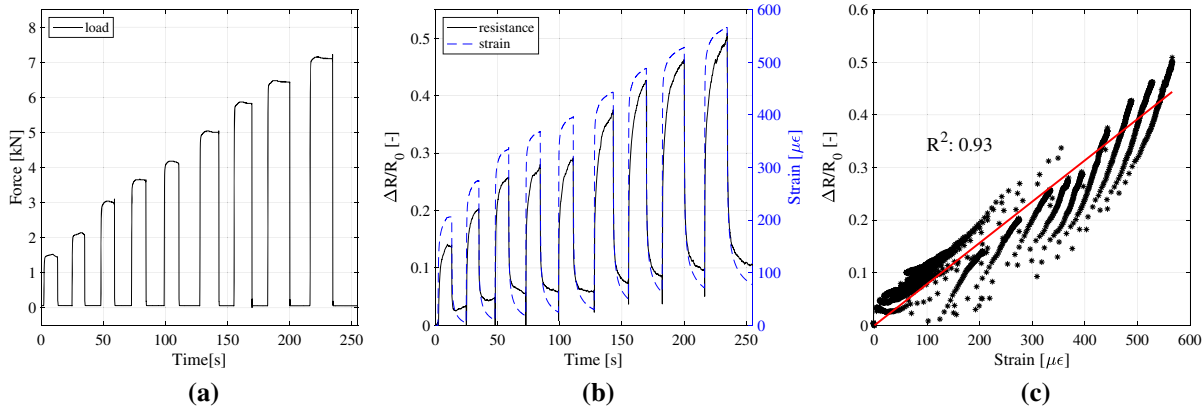

Fig. 10 Fast varying step load tests performed on slab sample: **a** load time history; **b** change of resistance and strain time histories; and **c** linear fit

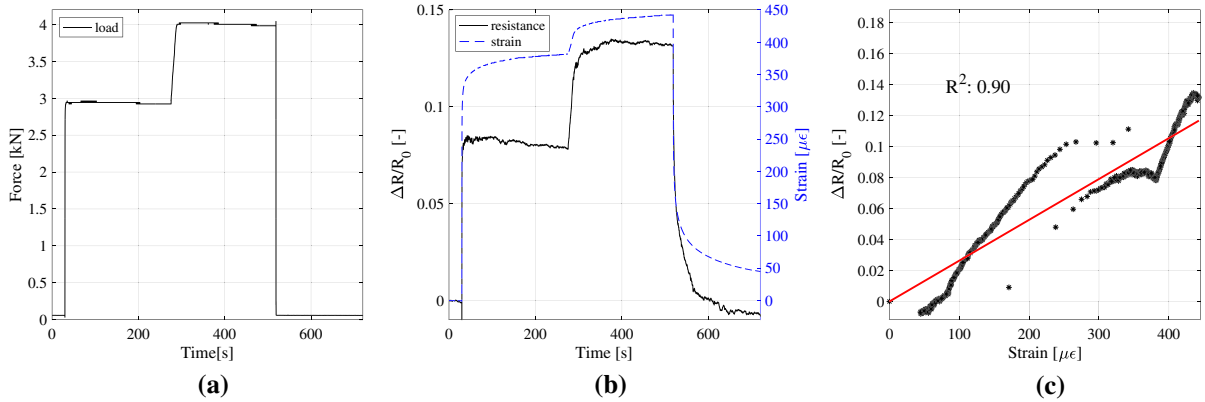

Fig. 11 Slow varying step load tests performed on slab sample; **a** load time history; **b** change of resistance and strain deformation time histories; and **c** linear fit

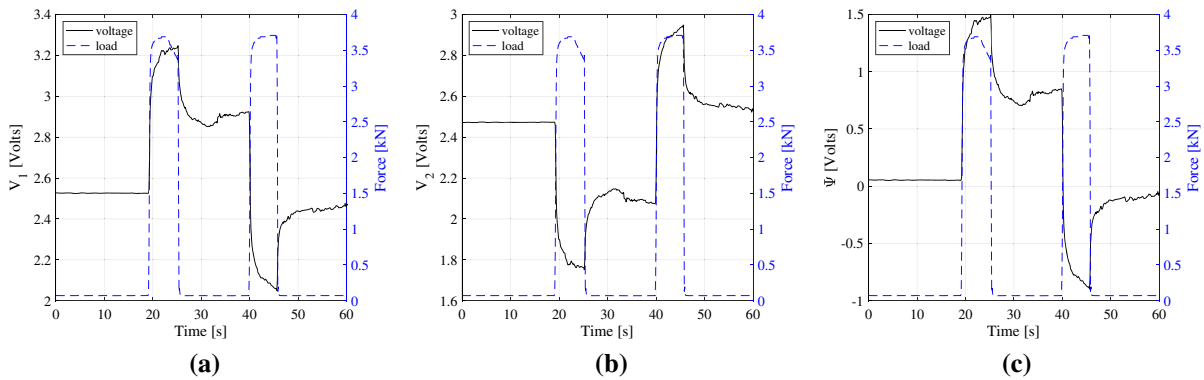

Fig. 12 Moving load test performed on slab sample; **a** load and voltage time history recorded from first half of sample volume; **b** load and voltage time history recorded from second half of sample volume; and **c** difference of both readings

present in off-the-shelf WIM systems. Being part of the pavement itself, the strain sensing pavement units is not prone to poor sensor-to-structure bonding and support an embedded deployment where the sensing

layer is covered by a protective surface, thus further increasing the durability against harsh environments.

The material is designed for optimum performance, and it is verified through experimental and analytical models. The mid-scale slab sample instrumented by tailored distributed line electrodes has been manufactured, and its capability of sensing the traffic loads has been preliminarily examined. According to the results, the induced deformation of the material and the variation in the electrical resistance measured between electrodes are highly linearly correlated. The slab sample generated WIM compatible signals during the tests enforcing the interest towards trials to be conducted on-site with a pavement sample of larger dimensions. The electrical outcomes have been found stable and suitable for sensing purposes. The sensing system operated at 5V DC. Therefore, energy demand is comparably low, and the system is rated to be easier to install in terms of hardware than other types of sensing systems available in the market. The novel composite showed promising performance in the small and medium scaled samples. The manufacturing of CMF-EVIzero composite requires only mechanical mixing; thus, this type of composite is particularly suitable for producing traffic load sensors also at large scales. Moreover, because of the eco-friendly nature of the EVIzero and usage of micro-sized carbon fibers, the environmental impact of the composite remains low.

This study is an initial first step towards fully operating WIM systems, aimed to develop and characterize a novel self-sensing composite material using small- and medium-scaled sensing elements in view of traffic monitoring applications. The promising results show that the material proposed in this paper could effectively serve efficient and sustainable traffic monitoring systems. Future field applications would require a tailored electrodes design, the development of an adequate electronic circuitry for data acquisition and transmission, and the development of a WIM algorithm and its implementation within a data storage and signal processing unit.

6 Conclusion

This paper presents the electrical and sensing investigations on a novel strain-sensing electrically conductive composite road pavement material suitable for WIM, newly developed and optimized in terms of mixture design. The fabrication steps are presented and precisely discussed. A series of tests on compacted cylindrical samples allows the identification of an electrical percolation region and a piezoresistive behavior that enhanced strain sensing capabilities. The optimized design is verified in terms of sensing performance, analytical model, and resistance readings. A slab sample of medium-scaled dimensions has been proposed and tested with rapid loading and slow loading tests in order to achieve a preliminary validation of the material in view of its application for WIM. According to the results, the slab sample can scale the amount of deformation by measuring the variations in the electrical resistance between the electrodes, thus allowing to detect the applied loads.

The noise produced by the sample is very low, and the electrical signals are stable. The moving load effects are observable on the outcome signals, which indicates the suitability of the proposed sensor system for low-cost and high durability WIM sensing for large-sized traffic monitoring. Future stages of the study will include field experiments with real vehicle loads and the investigation of the mechanical properties under changing environmental conditions.

Acknowledgements The authors would like to acknowledge the Horizon 2020 SAFERUP! Project leading these results.

Author contributions Following contributions are made by authors; conceptualization, FU and SL; methodology, HBB, AC and AD; software, HBB, AD; validation, AD, SL and FU; resources, FU; writing-original draft preparation, HBB; writing-review and editing, AC, AD, SL and FU; visualization, HBB and AD; supervision, SL and FU.

Funding This research has received funding from the European Union's Horizon 2020 research and innovation programme under SAFERUP! Project with Grant Agreement No. 765057.

Data availability The data is available upon a reasonable request.

Declarations

Conflict of interest The authors declare that they have no conflict of interest.

Ethics approval Not applicable.

Consent to participate Not applicable.

Consent for publication Not applicable.

References

1. Fiorillo A, Critello C, Pullano S (2018) Theory, technology and applications of piezoresistive sensors: a review. Sens Actuators A 281:156–175
2. Laflamme S, Ubertini F (2020) Back-to-basics: self-sensing materials for nondestructive evaluation. Mater Eval 78:526–536
3. Jeevanagoudar YV, Krishna RH, Gowda R, Preetham R, Prabhakara R (2017) Improved mechanical properties and piezoresistive sensitivity evaluation of MWCNTs reinforced cement mortars. Constr Build Mater 144:188–194
4. D'Alessandro A, Meoni A, Ubertini F, Materazzi AL (2018) Strain measurement in a reinforced concrete beam using embedded smart concrete sensors. In: Conference on Italian concrete days. Springer, pp 289–300
5. Shah S.P, Konsta-Gdoutos M, Metaxa Z, Mondal P (2009) Nanoscale modification of cementitious materials. In: Nanotechnology in construction, vol 3. Springer, pp 125–130
6. Han B, Ding S, Yu X (2015) Intrinsic self-sensing concrete and structures: a review. Measurement 59:110–128
7. Vaidya S, Allouche EN (2011) Strain sensing of carbon fiber reinforced geopolymer concrete. Mater Struct 44(8):1467–1475
8. Howser R, Dhonde H, Mo Y (2011) Self-sensing of carbon nanofiber concrete columns subjected to reversed cyclic loading. Smart Mater Struct 20(8):085031
9. Camacho-Ballesta C, Zornoza E, Garcés P (2016) Performance of cement-based sensors with CNT for strain sensing. Adv Cem Res 28(4):274–284
10. Hardy DK, Fadden MF, Khattak MJ, Khattab A (2016) Development and characterization of self-sensing CNF HPFRCC. Mater Struct 49(12):5327–5342
11. Pei C, Ueda T, Zhu J (2020) Investigation of the effectiveness of graphene/polyvinyl alcohol on the mechanical and electrical properties of cement composites. Mater Struct 53(3):1–15
12. Birgin HB, D'Alessandro A, Laflamme S, Ubertini F (2021) Hybrid carbon microfibers-graphite fillers for piezoresistive cementitious composites. Sensors 21(2):518
13. D'Alessandro A, Tiecco M, Meoni A, Ubertini F (2021) Improved strain sensing properties of cement-based sensors through enhanced carbon nanotube dispersion. Cem Concr Compos 115:103842
14. Chang L, Friedrich K, Ye L, Toro P (2009) Evaluation and visualization of the percolating networks in multi-wall carbon nanotube/epoxy composites. J Mater Sci 44(15):4003–4012
15. Feng C, Jiang L (2014) Investigation of uniaxial stretching effects on the electrical conductivity of cnt–polymer nanocomposites. J Phys D Appl Phys 47(40):405103
16. Dalla PT, Dassios KG, Tragazikis IK, Exarchos DA, Matikas TE (2016) Carbon nanotubes and nanofibers as strain and damage sensors for smart cement. Mater Today Commun 8:196–204
17. Feng C, Jiang L (2013) Micromechanics modeling of the electrical conductivity of carbon nanotube (cnt)–polymer nanocomposites. Compos A Appl Sci Manuf 47:143–149
18. Nikfar N, Zare Y, Rhee KY (2018) Dependence of mechanical performances of polymer/carbon nanotubes nanocomposites on percolation threshold. Physica B 533:69–75
19. Nayak S, Das S (2019) A microstructure-guided numerical approach to evaluate strain sensing and damage detection ability of random heterogeneous self-sensing structural materials. Comput Mater Sci 156:195–205
20. Aryanfar A, Medlej S, Tarhini A et al (2021) Elliptic percolation model for predicting the electrical conductivity of graphene–polymer composites. Soft Matter 17(8):2081–2089
21. Lee S-J, You I, Zi G, Yoo D-Y (2017) Experimental investigation of the piezoresistive properties of cement composites with hybrid carbon fibers and nanotubes. Sensors 17(11):2516
22. Dong W, Li W, Shen L, Sheng D (2019) Piezoresistive behaviours of carbon black cement-based sensors with layer-distributed conductive rubber fibres. Mater Des 182:108012
23. Zhang L, Ding S, Han B, Yu X, Ni Y-Q (2019) Effect of water content on the piezoresistive property of smart cement-based materials with carbon nanotube/nanocarbon black composite filler. Compos A Appl Sci Manuf 119:8–20
24. Wang H, Zhang A, Zhang L, Wang Q, Yang X, Gao X, Shi F (2020) Electrical and piezoresistive properties of carbon nanofiber cement mortar under different temperatures and water contents. Constr Build Mater 265:120740
25. Castañeda-Saldarriaga DL, Alvarez-Montoya J, Martínez-Tejada V, Sierra-Pérez J (2021) Toward structural health monitoring of civil structures based on self-sensing concrete nanocomposites: a validation in a reinforced-concrete beam. Int J Concrete Struct Mater 15(1):1–18
26. Birgin HB, D'Alessandro A, Laflamme S, Ubertini F (2020) Smart graphite-cement composite for roadway-integrated weigh-in-motion sensing. Sensors 20(16):4518
27. Downey A, D'Alessandro A, Laflamme S, Ubertini F (2017) Smart bricks for strain sensing and crack detection in masonry structures. Smart Mater Struct 27(1):015009
28. Meoni A, D'Alessandro A, Kruse R, De Lorenzis L, Ubertini F (2021) Strain field reconstruction and damage identification in masonry walls under in-plane loading using

dense sensor networks of smart bricks: Experiments and simulations. Eng Struct 239:112199
29. Downey A, D'Alessandro A, Ubertini F, Laflamme S, Geiger R (2017) Biphasic dc measurement approach for enhanced measurement stability and multi-channel sampling of self-sensing multi-functional structural materials doped with carbon-based additives. Smart Mater Struct 26(6):065008
30. Birgin HB, Laflamme S, D'Alessandro A, Garcia-Macias E, Ubertini F (2020) A weigh-in-motion characterization algorithm for smart pavements based on conductive cementitious materials. Sensors 20(3):659
31. Corecom: EVIzero technical standards. https://www.evizero.com/download/technical-standards-of-contract-rev-01.pdf. Accessed 7 Apr 2022
32. SGL Carbon: Sigrafil short carbon fibers. https://www.sglcarbon.com/en/markets-solutions/material/sigrafil-short-carbon-fibers. Accessed 25 Feb 2021
33. Corecom: Caratterizzazione sperimentale dei leganti trasparenti cores evizero per applicazioni in ambito stradale. https://www.evizero.com/download/caratterizzazione-sperimentale.pdf. Accessed 25 Feb 2021
34. EN C (2007) 12697-31, bituminous mixtures-test methods for hot mix asphalt-part 31: Specimen preparation by gyratory compactor. European Committee For Standardization
35. EN B (2004) 12697-33: Bituminous mixtures. Test methods for hot mix asphalt. Specimens prepared by roller compactor. British Standards Institution, London
36. McDonald KT (2019) Resistance of a disk. https://www.hep.princeton.edu/~mcdonald/examples/resistivedisk.pdf. Accessed 20 Sept 2021
37. Pan N (1993) A modified analysis of the microstructural characteristics of general fiber assemblies. Text Res J 63(6):336–345
38. Kumar V, Rawal A (2016) Tuning the electrical percolation threshold of polymer nanocomposites with rod-like nanofillers. Polymer 97:295–299
39. García-Macías E, D'Alessandro A, Castro-Triguero R, Pérez-Mira D, Ubertini F (2017) Micromechanics modeling of the uniaxial strain-sensing property of carbon nanotube cement-matrix composites for SHM applications. Compos Struct 163:195–215